Ceramics International 51 (2025) 16951–16958

Contents lists available at ScienceDirect

Ceramics International

journal homepage: www.elsevier.com/locate/ceramint

Eu^{3+}-doped Laponite as a new probe for combined confocal Raman imaging fluorescence

Nerea Iturrioz-Rodríguez [a,1], Rosa Martín-Rodríguez [a,b], Fernando Aguado [a,c], Lorena González-Legarreta [a,b], Jesús González [a,c], Rafael Valiente [a,d], Mónica L. Fanarraga [a,e], Ana C. Perdigón [a,b,*]

[a] Nanomedicine Group, IDIVAL, Avda. Cardenal Herrera Oria s/n, 39011, Santander, Spain
[b] QUIPRE Department, Universidad de Cantabria, Avda. de Los Castros, 46, 39005, Santander, Spain
[c] CITIMAC Department, Universidad de Cantabria, Avda. de Los Castros, 48, 39005, Santander, Spain
[d] Applied Physics Department, Universidad de Cantabria, Avda. De Los Castros, 48, 39005, Santander, Spain
[e] Molecular Biology Department, Universidad de Cantabria, Avd. Cardenal Herrera Oria s/n, 39011, Santander, Spain

ARTICLE INFO

Handling Editor: Dr P. Vincenzini

Keywords:
Fluorescence
Confocal Raman imaging
Laponite
Europium
Nanoclay

ABSTRACT

Laponite is a synthetic nanoclay highly attractive for medical applications, particularly as a platform for drug delivery and as an active material or bioimaging. The use of fluorescent dyes or even the functionalization of the nanoplatforms is a common practice to visualize the nanosystem within cell structures. However, these practices involve indirect characterization methods or could induce irreversible effects on the nanoparticle-cell interaction. Here, we introduce a methodology combining luminescence and confocal Raman microscopy to track the nanosystem and detect its cargo independently, using Eu^{3+} as a fluorescent probe. Confocal Raman microscopy allow us to determine the localization of the nanoparticle by its unique Raman spectrum fingerprint while mapping the cell. At the same time, Eu^{3+} luminescence serves to detect the cargo by its emission spectrum. Speciffically, we describe here the use of Eu-doped Laponite as a fluorescent probe, to track its uptake and incorporation into a macrophage cell line. To discard potential adhesion to the cell membrane, images were taken at different Z planes. In this way, we have observed that the cargo remains attached to the nanoparticle. Finally, the biocompatibility of the nanoplatforms and their cargo has been studied, showing no significant difference in the survival rate.

1. Introduction

Laponite, a synthetic nanoclay, holds high potential for biomedical applications due to its precisely controlled chemical composition. Characterized by disc-shaped particles and a remarkable aspect ratio, Laponite particles typically measure around 25 nm in diameter and 0.92 nm in thickness. Electrostatic forces facilitate the attraction between these discs, causing them to stack together in solid state. Since Laponite can swell under specific experimental conditions, it can delaminate in water, forming a stable colloidal dispersion [1]. Thus, this exfoliated form of Laponite is an ideal candidate to be applied in cell therapy, diagnosis, and bioimaging [2]. In addition, its particular rheology is of interest in its use as a component in hydrogel/scaffolds and as a nano-platform for drug delivery utilizing ion exchange reaction.

Moreover, Laponite is a versatile and non-toxic nanomaterial that has inspired numerous ways to design biomaterials for biomedical applications. In particular, Laponite has been declared an active material showing its efficiency in bone tissue regeneration. Additionally, in the last decades, various nanohybrid materials made of Laponite have attracted scientific interest, due to their unusual and synergetic physicochemical properties, which can not be achieved by a single material [3]. In particular, Wang et al. developed an approach to easily encapsulate the antibiotic amoxicillin within Laponite-doped nanofibers, showing a maintained release of the drug, cytocompatibility, and antimicrobial activity toward the growth inhibition of a model bacterium of *Staphylococcus aureus* [4]. Laponite, with chemical formula

This article is part of a special issue entitled: PRE'24 published in Ceramics International.

* Corresponding author. Nanomedicine Group, IDIVAL, Avda. Cardenal Herrera Oria s/n, 39011, Santander, Spain.
E-mail address: perdigonac@unican.es (A.C. Perdigón).
[1] Current affiliation: Cellular Oncology Group, Biogipuzkoa Health Research Institute, San Sebastian, Spain.

https://doi.org/10.1016/j.ceramint.2025.02.246
Received 20 September 2024; Received in revised form 16 January 2025; Accepted 18 February 2025
Available online 20 February 2025

$Na_{0.7}[Si_8Mg_{5.5}Li_{0.3}O_{20}(OH)_4]$, consists of one sheet of octahedral magnesia units covered by two tetrahedral SiO_4based sheets, in which isomorphic substitutions of Mg^{2+} by Li^+ in the octahedral sheet confers a permanent negative layer charge. This layer charge is compensated by exchangeable hydrated Na^+ cations in the interlayer space, balancing out the overall charge. In this kind of nanomaterials, the drug is first encapsulated through a reversible intercalation process, which consists of the insertion of guest species into two-dimensional host materials and, consequently, by the Na^+ exchange [5].

The development of new materials combining lanthanide ions and different host matrices holds great potential for application in sensing, in particular as new fluorescent probes for biomedical applications [6]. The trivalent europium ion (Eu^{3+}) is particularly interesting because it exhibits intense red emission not only in crystalline hosts, but also surrounded by organic ligands [7]. Specifically, Eu^{3+} ions show sharp band emissions, low toxicity, biocompatibility, and high photostability. As an example, europium-doped fluoroapatite nanorods have been proposed as cell imaging biomaterial and anticancer drug carriers [8].

In nanomedicine, it is a common practice to use fluorescent dyes for labeling the nanomaterial to follow its entrance into the cell through confocal fluorescence microscopy. However, this indirect method implies nanoparticle functionalization or the use of fluorescent dyes to allow the visualization and localization of the nanomaterial into the cell structures, cytosol, or cell nuclei, which could irreversibly affect the nanoparticle-cell interaction. To solve this issue, we have recently applied a free-label non-invasive methodology based on the confocal Raman microscopy (CRM) technique, to track the uptake of Laponite nanoparticles into a macrophage cell line without the need for a luminescent probe [9]. Indeed, Raman spectroscopy is a powerful technique for cell imaging, which can accurately determine the chemical and compositional properties of biological material [10]. Moreover, the integration of Raman spectroscopy with confocal microscopy allows the precise placement of the nanoparticle by its unique Raman spectrum fingerprint by mapping the cell.

We present here as a step forward, a combined luminescence and CRM to follow the nanosystem and independently detect the cargo. For this purpose, we have used Eu-doped Laponite as a proof of concept to monitor the absorption and internalization of Laponite nanoparticles into the J774 macrophage cell line. The acquisition of the Raman signal from the nanoparticle and the cell, and Eu^{3+} luminescence acquired in the same spot, can identify the localization of the nanoparticle and Eu^{3+} ions separately inside the cell. Eu^{3+} ions serve as the cargo, which could be replaced with a (fluorescent) drug, and Laponite as the drug delivery system. Firstly, Eu-doped Laponite nanoparticles have been morphologically characterized -size and shape-by transmission electron microscopy (TEM). The Eu^{3+} ions exchange process has been followed by X-ray diffraction (XRD) and thermogravimetry (TG) measurements. Subsequently, after functionalization with serum, Eu-doped Laponite particles were administrated to a culture of macrophages, and the nanodispenser and the cargo were independently followed by Luminescence and Raman spectroscopy inside the cell. Finally, the biocompatibility of the nanoplatforms and their cargo has been studied by analyzing the survival of the macrophages after 24, 48, 72, and 96 h of exposure to Laponite and Eu-doped Laponite.

2. Material and methods

2.1. Synthesis and characterization of the Eu-doped laponite

Laponite provided by BYK-Chemie GmbH was firstly doped with Eu^{3+} cations via a cation exchange reaction as follows: 300 mg of clay were dispersed in 25 mL of a 2.5 cation exchange capacity (CEC) of Eu (NO_3) solution for 24 h. This procedure was repeated an additional three times. The sample was thoroughly washed with deionized water, recovered by centrifugation, and dried. The characterization of the samples was performed using TEM (JEOL JEM 1011 microscope), XRD (Bruker D8 Advance diffractometer), and TG (Setaram Setsys Evolution 1700). For TEM measurements the powder was suspended in water and a drop was deposited on a carbon-coated copper grid. XRD patterns were recorded using Cu Kα radiation over the 1.5°–70° 2θ range with 0.03° steps and a counting time of 30s per step.

For TG analysis, the sample was heated in air using an open platinum crucible, starting from room temperature and increasing to 1000 °C at a rate of 10 °C per minute. The water vapor signal was monitored with a Pfeiffer OmniStar Prisma mass spectrometer (MS) connected to the TG apparatus.

Emission spectra were recorded in a FLSP920 spectrofluorometer (Edinburgh Instrument), equipped with a continuous-wave 450 W Xe lamp and double monochromators in emission and excitation.

Raman measurements and luminescence spectra within cells were conducted using a JASCO NRS-4500 Confocal Raman Microscope, utilizing a 532 nm excitation wavelength. The light was captured with a 100x objective, dispersed using 900 grooves/mm grating, and detected by an Andor Newton CCD detector that is Peltier-cooled.

2.2. Cell culture and confocal Raman spectroscopy

J774 A1 murine macrophage cells (from ATCC) were cultured under standard conditions in Iscove's Modified Dulbecco's Medium (IMDM, from Gibco, Thermo Fisher Scientific, ref: 12440053) containing 10 % fetal bovine serum (FBS) and antibiotics (from Gibco, Thermo Fisher Scientific). First, the nanosystem was functionalized with FBS for better cell uptake. Briefly, 200 μg/mL of Laponite or Eu-doped Laponite was resuspended in 30 % FBS by mild probe sonication (3–5 cycles, at a frequency of 20 kHz) in a SONICS Vibra-Cell VCX130 Ultrasonic Processor (Sonics & Materials INc). After, the aggregates of Laponite were removed by centrifugation (1000 rpm for 15 min). For Raman spectroscopy, cells were cultured on CaF_2 coverslips for 24 and 48 h to prevent overlapping Raman peaks from standard glass slides with the cells and Laponite. The cells were then fixed using 10 % neutral buffered formalin (approximately 4 % formaldehyde) from Sigma-Aldrich (ref: HT501128-4L). After drying, the samples were analyzed using the Jasco NRS 4500 spectrometer. The spectra were analyzed using Spectra Manager™ software from JASCO. Upon obtaining the Raman spectra, the peak at 684 cm^{-1} (corresponding to the Laponite peak) and the band between 580 and 635 nm (representing Europium fluorescence) were selected for analysis at each acquisition point. For each spectrum, baseline correction was applied to remove background noise, and the integrated intensity (the area under the curve) was calculated within the specified range. These integrated intensities were then mapped to their respective spatial positions, forming a grid of values. The resulting values were converted into a 2D image, where colour intensities represent the distribution of peak intensity, producing a heatmap-like image, with each pixel's colour corresponding to the integrated intensity at that location.

2.3. Cell viability

The viability of macrophages was assessed by quantifying necrotic cells using Trypan Blue dye (from Sigma Aldrich, ref: T8154). This assay specifically measures cell membrane integrity by allowing the dye to penetrate only non-viable cells, thereby providing a direct and quantitative indicator of cell death. Cell counts were performed with the TC20™ Automated Cell Counter (from Bio-Rad). Epifluorescence images of control and Eu-doped Laponite cells were taken with the ZOE Fluorescent Cell Imager (BIO-RAD, Ref 1450031) after 24, 48, 72 and 96 h of 200 μg/mL Laponite or Eu-doped Laponite exposure.

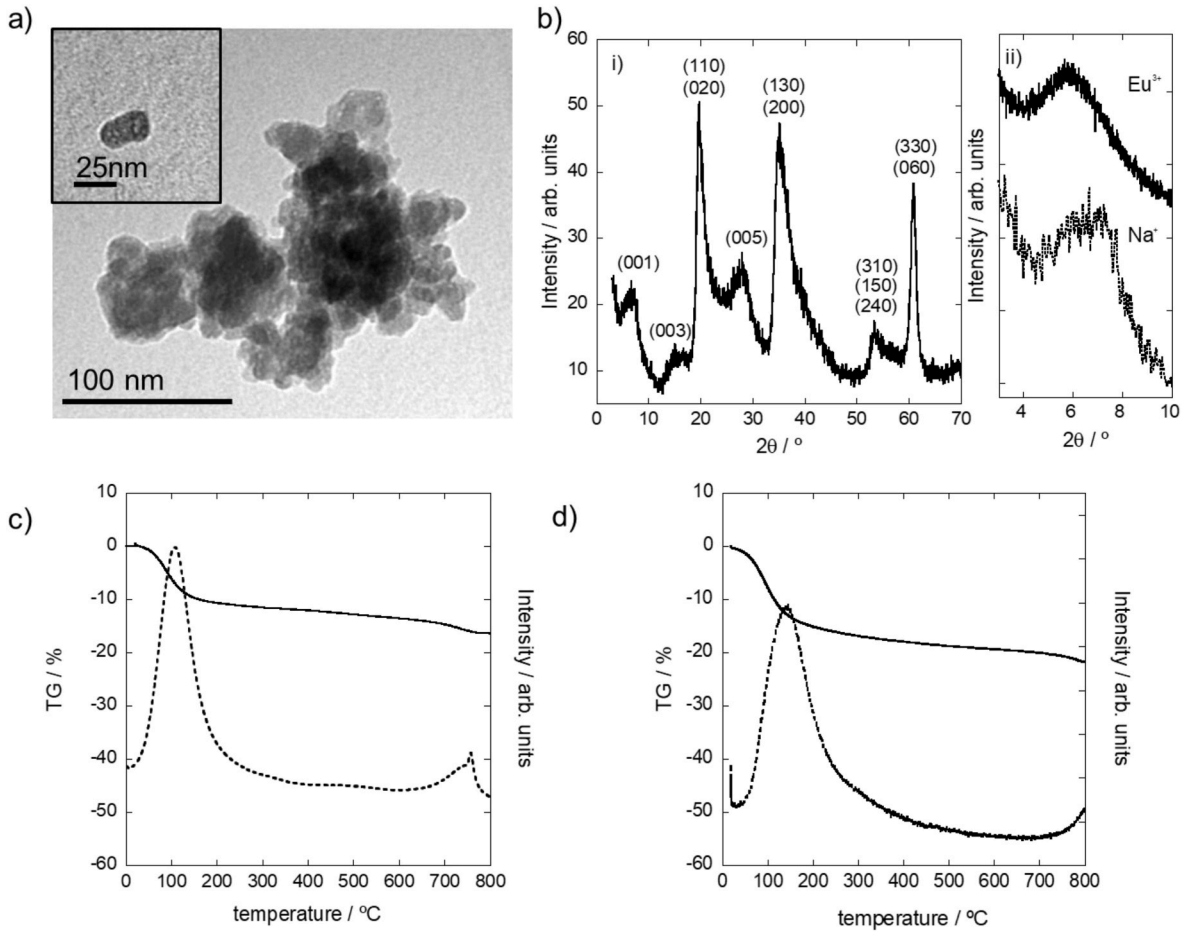

Fig. 1. a) Representative TEM image of Eu-doped Laponite; b) XRD pattern of Laponite i) and comparison of the (001) reflection of Laponite before and after exchange with Eu ii); c) Representative TG curve (solid line) and water signal by MS of Laponite (dashed-line); d) Representative TG curve (solid line) and water signal by MS of Eu-doped Laponite (dashed-line).

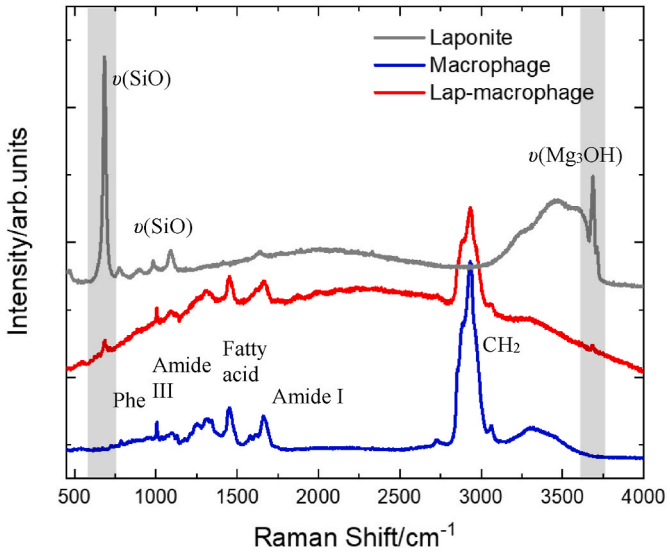

Fig. 2. Representation of the Raman spectra of laponite (grey), a macrophage (blue), and Laponite after the incubation with cells (red). The characteristic peaks of Laponite, at around 684 cm^{-1} and 3688 cm^{-1}, can be observed in the intracellular Laponite. (For interpretation of the references to colour in this figure legend, the reader is referred to the Web version of this article.)

3. Results and discussion

3.1. Laponite/Eu-doped laponite characterization

Eu^{3+} cations were firstly incorporated in the Laponite particles by cation exchange reaction, and subsequently, the nanoplatforms and their cargo were independently characterized by emission and Raman spectroscopy. It is important to point out that the replacement of Na^{+} by Eu^{3+} cations has no impact on the stability and functionality of Laponite, since the interaction of the interlayer cations with the clay structure is electrostatic in nature. Fig. 1 (a) shows transmission electron micrographs of the Eu-doped Laponite sample where it is worth noticing the morphologic homogeneity, the hexagonal shape, and the nanometric size of the particles. The layered structure is also evidenced by X-ray diffraction (see Fig. 1b). The XRD pattern of pristine laponite is characterized by general and basal reflections, typical of swelling clays. The symmetrical basal (001) reflection corresponds with the basal spacing, related to the distance between layers. It can be observed, that upon intercalation, the basal spacing increased notably from around 1.3 nm–1.5 nm, indicating that the interlayer Na^{+} ions were replaced by Eu^{3+} cations. The TG and water signal curves of Laponite and Eu-doped Laponite are presented in Fig. 1 ((c) and (d)). The TG curves show a mass loss step up to 175 °C which coincides with a maximum in the water signal in both samples. This mass loss is related to the adsorbed and interlayer water in clay minerals, being ~10 % in Laponite and ~14 % in Eu-doped Laponite. The difference in those values reflects the hydration enthalpy of both cations, −406 kJ/mol for Na^{+} cations and −3612 kJ/

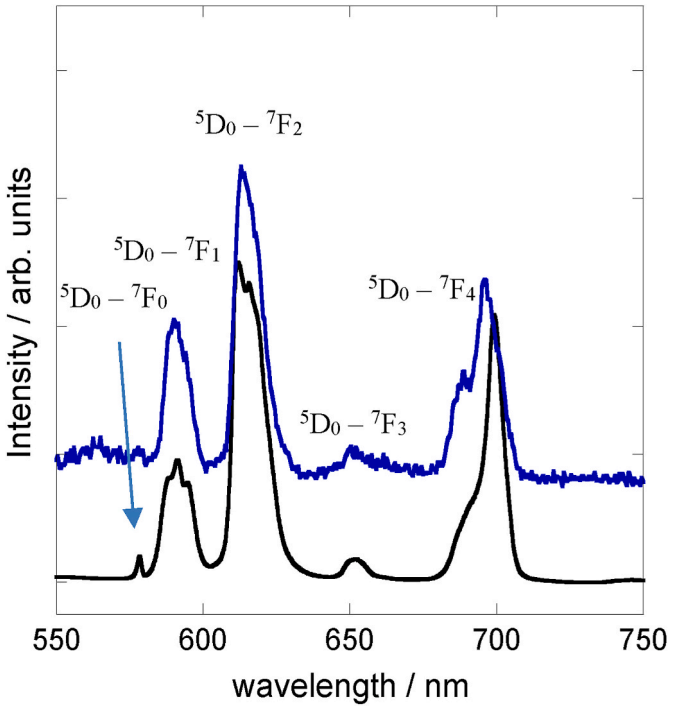

Fig. 3. Eu^{3+} luminescence spectrum upon excitation at 393 nm Eu-doped Laponite in powder form (black) and as a 5 mg/mL suspension in FBS medium (blue). (For interpretation of the references to colour in this figure legend, the reader is referred to the Web version of this article.)

mol for Eu^{3+} cations, confirming the incorporation of Eu^{3+} cations in the Laponite after the cation exchange process.

3.2. Cellular uptake of Eu-doped laponite

One important aspect of the study of nanocarriers as drug delivery systems is to confirm the intracellular uptake of the nanomaterial and its cargo. This is usually done by indirect methods such as confocal fluorescence microscopy, attaching a fluorescent label to the nanoparticles. This approach has some drawbacks, including the assumption that the dye is still attached to the nanosystem when it is uptaken by the cell, and thus, the localization of the dye is the same as the nanomaterial and its cargo. Here, we present a combination of Raman spectroscopy and fluorescence that allows for the independent localization of the nanocarrier and its fluorescent cargo, differentiating whether only the nanomaterial or both the nanomaterial and the therapeutic agent have reached the target. As mentioned in the introduction, we use Laponite as an example of a drug delivery system, exchanged with Eu^{3+} as a proof of concept of a therapeutic agent due to its fluorescence. For that, 200 μg/mL of Laponite was administrated to macrophages and analyzed after 24 h.

Firstly, Fig. 2 includes the Raman spectrum of Laponite (grey) where principal contributions are indicated. An exhaustive analysis of all the peaks that appear in the spectrum can be found elsewhere, thus we have assigned only the most intense peaks in the figure [9]. Laponite Raman spectrum has two principal regions, the layer structure region (up to 1200 cm^{-1}) and the hydroxyl stretching region (3550-3750 cm^{-1}). A weak band at ~1095 cm^{-1} and the most intense band situated at ~684 cm^{-1}, both in the low wavenumber vibrational region, are attributed to

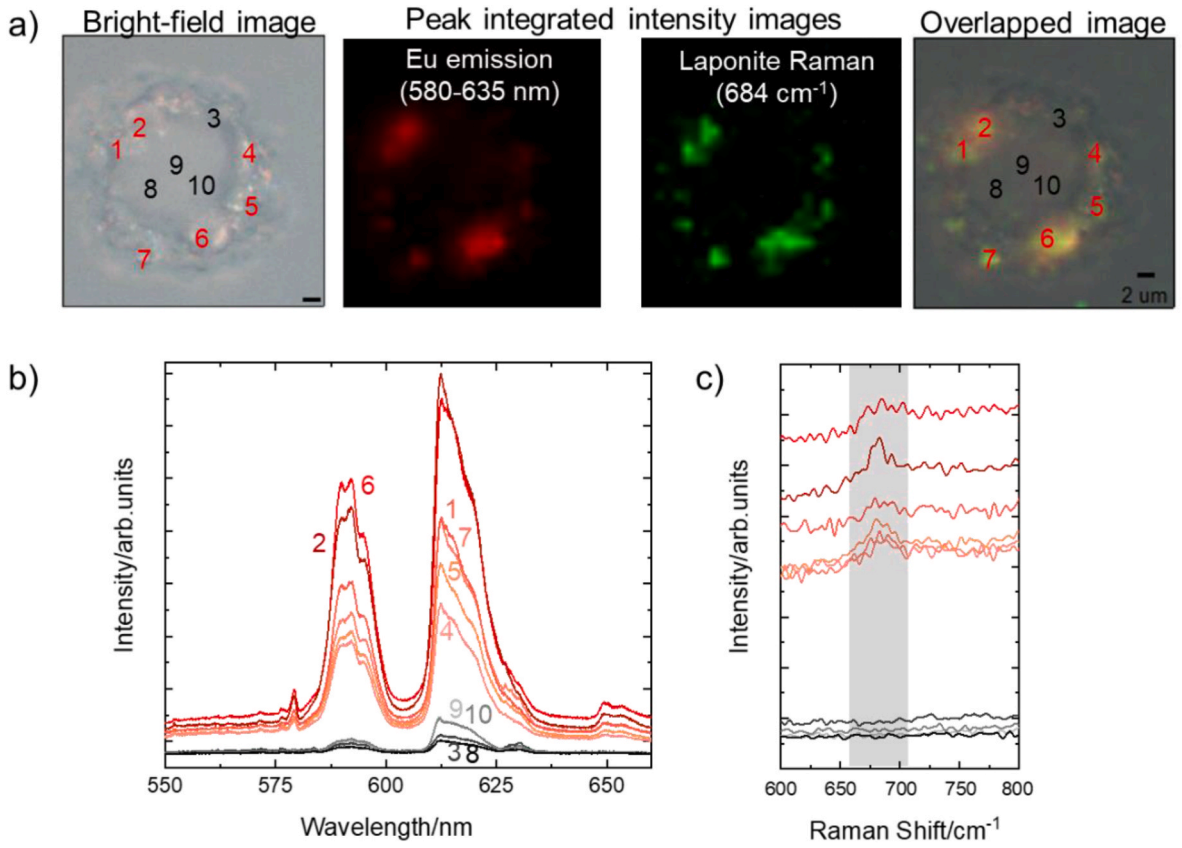

Fig. 4. a) Bright-field image of a macrophage 24 h after the administration of Eu-doped Laponite (scale bar: 2 μm). Peak integrated intensity images of the 580–635 nm bands (in red) corresponding to the fluorescence of europium, and 684 cm^{-1} peak (in green) corresponding to the Raman signal of Laponite. The image on the right shows the overlay of the previous three images; b) Ten examples of luminescence spectra indicating the presence of Eu-doped Laponite within the macrophage (points 1, 2, 4, 5, 6, 7) as well as areas without Laponite (point nº 3, 8, 9, 10), and c) Raman spectra of the different points displaying the peak associated with Laponite at 684 cm^{-1}. (For interpretation of the references to colour in this figure legend, the reader is referred to the Web version of this article.)

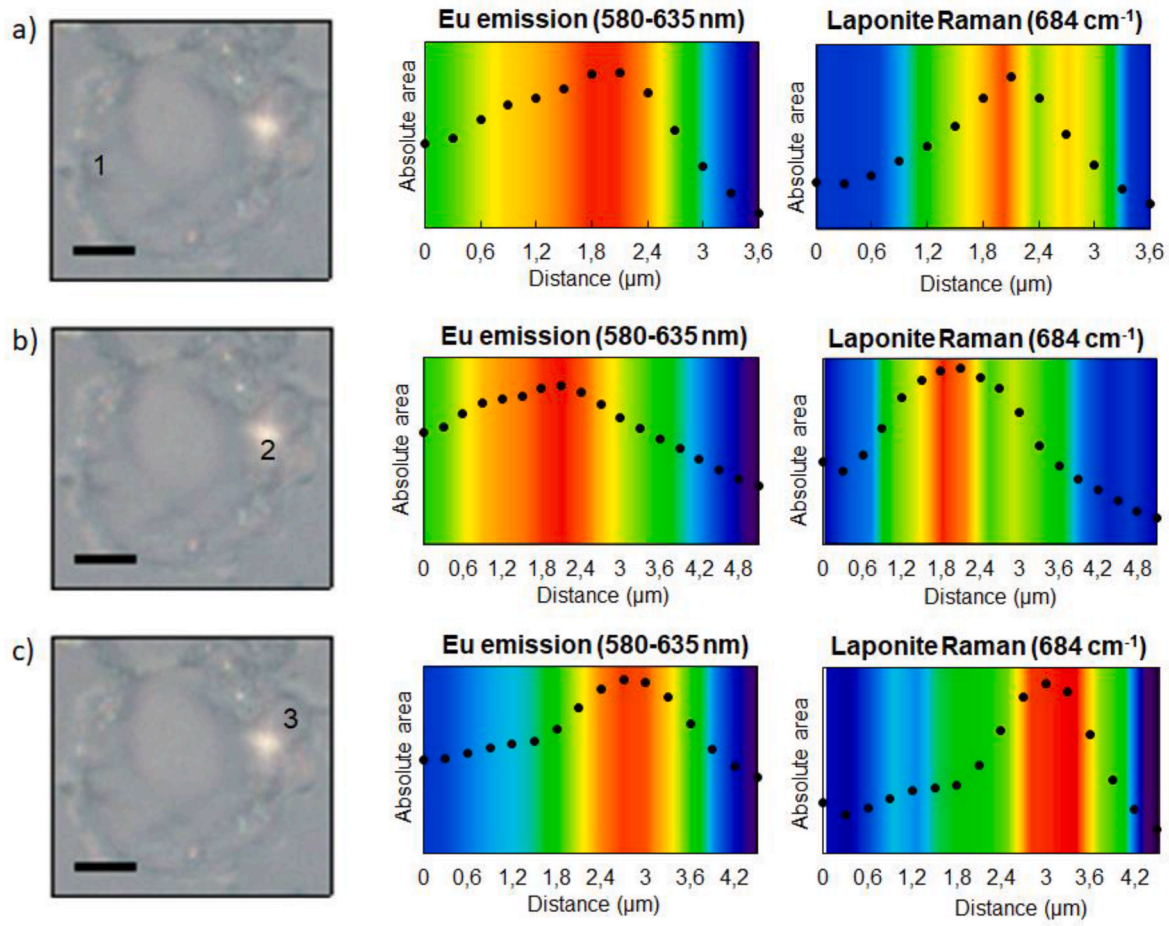

Fig. 5. a) Bright-field image of a macrophage after 24 h of the Lap-Eu administration (scale bar 5 μm) indicating one point where different confocal planes have been taken. The graph in the middle shows the integration luminescence intensity of the 580–635 nm band (europium) and the graph on the right shows the integration intensity of laponite Raman peak at 684 cm^{-1} at the different Z planes; b) and c) represent two more points that represent other Z planes.

the asymmetric and symmetric stretching mode, υ(SiO), of the SiO_4 tetrahedra [11]. In the hydroxyl stretching region, the most characteristic sharp peak at ~3680 cm^{-1} is attributed to the υ(Mg_3OH) vibrations in the octahedral sheet [12]. The two more intense Laponite signals previously identified at ~684 cm^{-1} and ~3680 cm^{-1} (highlighted in grey in Fig. 2), will serve to probe the nanoparticle uptake inside the cell. Fig. 2 also includes representative Raman spectra of a macrophage (blue) and a macrophage after exposure to Laponite for 24 h (red). Despite the complex nature of biological samples, Raman spectroscopy has become a useful technique to study cell chemical structures via their vibrational fingerprint. Indeed, some peaks correspond to cellular structures in the red and blue spectra, including signals attributed to proteins: The peak at ~1000 cm^{-1} is adscribed to the aromatic amino acid Phenylalanine [13,14], the peak at ~ 1260 cm^{-1} to the amide III (α-helix or random) [12–16], and the α-helix amide I to the peak at 1655 cm^{-1} [17]. Also, bands related to lipids such as the typical band at 1440 cm^{-1} of fatty acids [13], and the vibrational stretching region of the hydrocarbon chain structure (CH_2) at 2850 cm^{-1} [18], can be observed. After Laponite administration, the characteristic peaks of the silicate at 684 cm^{-1} and 3680 cm^{-1} can be identified in the macrophage spectrum. Thus, as we have previously reported, Raman spectroscopy can also provide direct information about the localization of the nanoplatforms *in situ* without the need for any other labeling technique [9,19,20]. Additionally, it allows for the detection of encapsulated cargo within the nanocarrier, as long as the signals of the different components of the nanosystem do not overlap. In this sense, Matthäus et al. have also utilized Raman spectroscopy to analyze the cargo inside nanocarriers. This study demonstrated that Raman spectroscopy is an effective tool for examining the uptake of β-carotene loaded into polymeric nanoparticles [21].

Secondly, we carried out cargo detection of the Eu^{3+}cations inside Laponite particles by photoluminescence. For this purpose, 200 μg/mL of Eu-doped Laponite was administrated to macrophages. The emission spectra of Eu^{3+} in Eu-doped Laponite, excited at 393 nm, were previously examined both in powder form and as a suspension in FBS. These findings are illustrated in Fig. 3.

The peaks observed in the luminescence spectrum correspond to transitions from the $^5D_0$ excited state to low energy lying ^7F_J (J = 1–4). Each transition displays a characteristic emission band at approximately 590, 617, 653, and 700 nm, respectively, with the $^5D_0 \rightarrow {}^7F_2$ transition responsible for the predominant red emission [7]. Eu^{3+} luminescence in Laponite suspended in FBS is comparable to powder form, regarding emission bandwidth and intensity ratio of the different bands.

Afterwards, we investigated the photoluminescence and Raman spectra of macrophages following 24 and 48 h of exposure to Eu-doped Laponite.

Fig. 4a displays a bright-field image of a macrophage, marking the points (numbered 1 to 10) where the luminescence emission and Raman spectra depicted in Fig. 4b and c respectively, are showcased. The subsequent two images illustrate the peak-integrated intensity images acquired after cell mapping, revealing the relative intensity of specific bands of Eu^{3+} emission at 580–635 nm (in red) and the Raman peak of Laponite at 689 cm^{-1} (in green), in those selected 10 points. The red and green dots, corresponding to the Eu^{3+} cargo and the Laponite

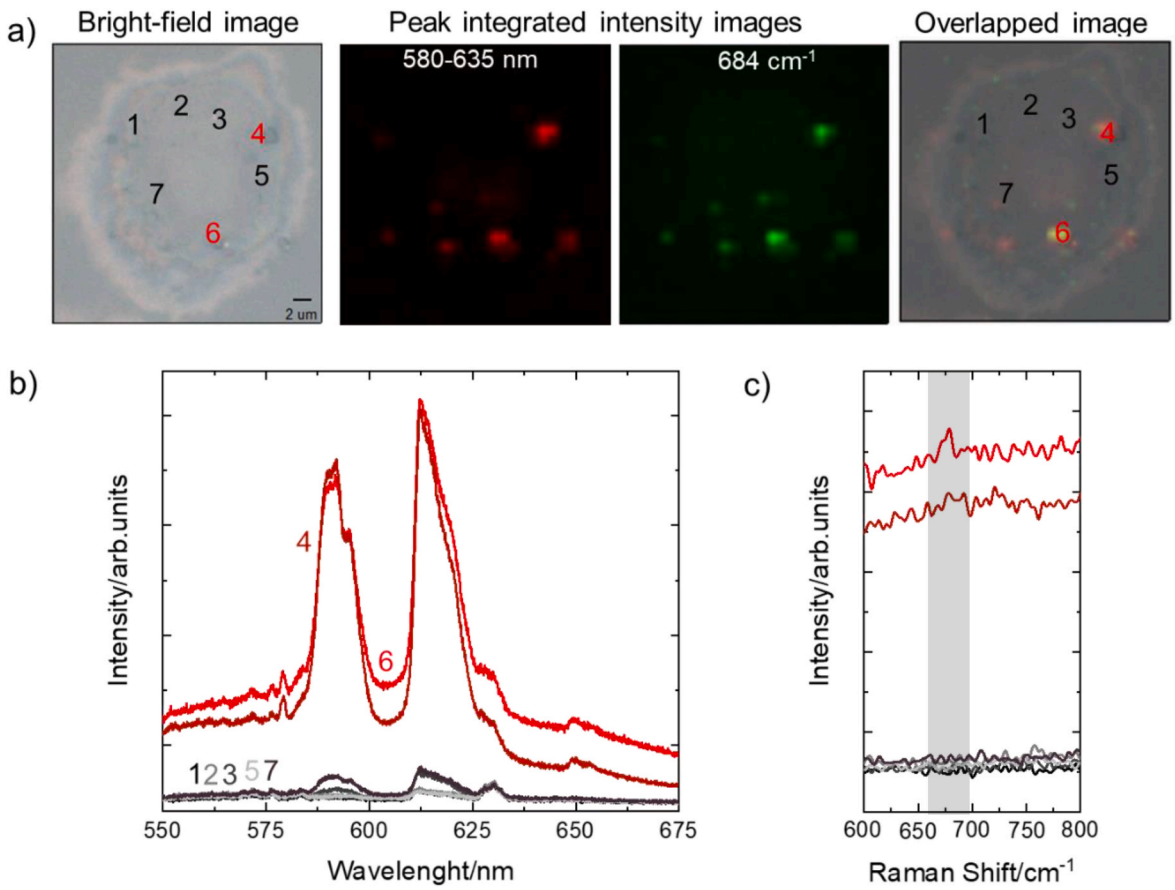

Fig. 6. a) Bright-field image of a macrophage 48 h after administration of Eu-doped Laponite (scale bar 2 μm). Peak integrated intensity images of the 580–635 nm bands (in red) correspond to the fluorescence of Eu^{3+}, and the 684 cm^{-1} peak (in green) corresponds to the Raman signal of Laponite. The image on the right shows the overlap of the previous three images; b) Seven examples of luminescence spectra indicating the presence of Eu-doped Laponite inside the macrophage (points 4 and 6) and areas without the Laponite (points nº 1, 2, 3, 5, and 7); and c) the Raman spectra of the different points showing the peak related to the Laponite at 684 cm^{-1}. (For interpretation of the references to colour in this figure legend, the reader is referred to the Web version of this article.)

nanoplatform, respectively, can be unequivocally identified in the images, providing a clear and independent localization of both systems within the cell. Points 1, 2, 4, 5, 6, and 7 appear in red and green colors in the images, confirming the presence of Eu-doped Laponite in these locations. By contrast, points 3, 8, 9, and 10 remain uncolored, suggesting the absence of Eu-doped Laponite particles in these areas of the macrophage. As verified in the overlapped image, the emission of Eu^{3+} coincides with the Raman peak of Laponite, indicating a long-term association between Eu^{3+} and Laponite at physiological conditions. This alignment suggests that Eu^{3+} remains linked to the Laponite structure. The numbers included in the bright-field image correspond to the fluorescence and Raman spectra represented in Fig. 4b. The luminescence spectra shown in Fig. 4b indicate areas in the cell with high intensity of Eu^{3+} emission (in red). At the same time, other regions exhibit almost no intensity (in black/grey), thus allowing us to determine the location of the cargo (Eu^{3+}) within the cell. Similarly, the integrated intensity of the Raman peaks (Fig. 4c) indicates the localization of the nanoplatforms. Interestingly, points that had a high Eu^{3+} luminescence intensity, exhibited as well, the characteristic Raman peak at 684 cm^{-1} corresponding to Laponite, demonstrating that Laponite and Eu^{3+} co-localized in the cell.

To verify that the signals of Laponite and Eu^{3+} originated from inside the cell, rather than from potential adhesion to the cell membrane, we captured images at different Z planes with 300 nm intervals at three specific points within a single cell. Fig. 5a, b, and c show these three spots. The integrated intensity of the luminescence emission band at 580–635 nm (middle) and the Raman peak at 684 cm-1 (right) at each focal distance are represented in the Figure. The band intensity is not constant over the different Z-planes, being more intense in the ones situated in a distance range of 1.8–2.7 μm from the focus. Indeed, these distances correspond to the middle planes of the cells, suggesting that both, Eu^{3+} and Laponite are inside the cell. Furthermore, as both luminescence and Raman intensities overlap in the same Z planes, it can be concluded that Eu^{3+} is attached to the Laponite particle.

Moreover, to confirm that this methodology is suitable for longer experiments, we analyzed the Raman spectra and luminescence emission of macrophages 48 h after the administration of Eu-doped Laponite. As expected, there is a lower amount of nanoparticles due to the division of macrophage. Fig. 6 shows the bright-field image highlighting the spots (numbered 1 to 6) represented in Fig. 6b and c. Similarly that in Fig. 5, the integrated intensity images of the Eu^{3+} emission correlate with the integrated intensity of the Raman 684 cm^{-1} peak of Laponite. Even after 48 h of Eu-doped Laponite administration, we can still distinguish both intensities in the macrophage. As introduced earlier, although the amount of Laponite and Eu^{3+} has decreased in the cells due to the macrophage division, both signals are still detectable and overlay, indicating that Eu^{3+} might still be attached to Laponite over time.

3.3. *Biocompatibility of Eu-doped laponite*

Finally, the biocompatibility of the nanoplatforms and the cargo has been studied by analyzing the survival of the macrophages after 24, 48, 72, and 96 h of exposure to 200 μg/mL. As Fig. 7a shows, there are no statistical differences in the survival percentage of control cells

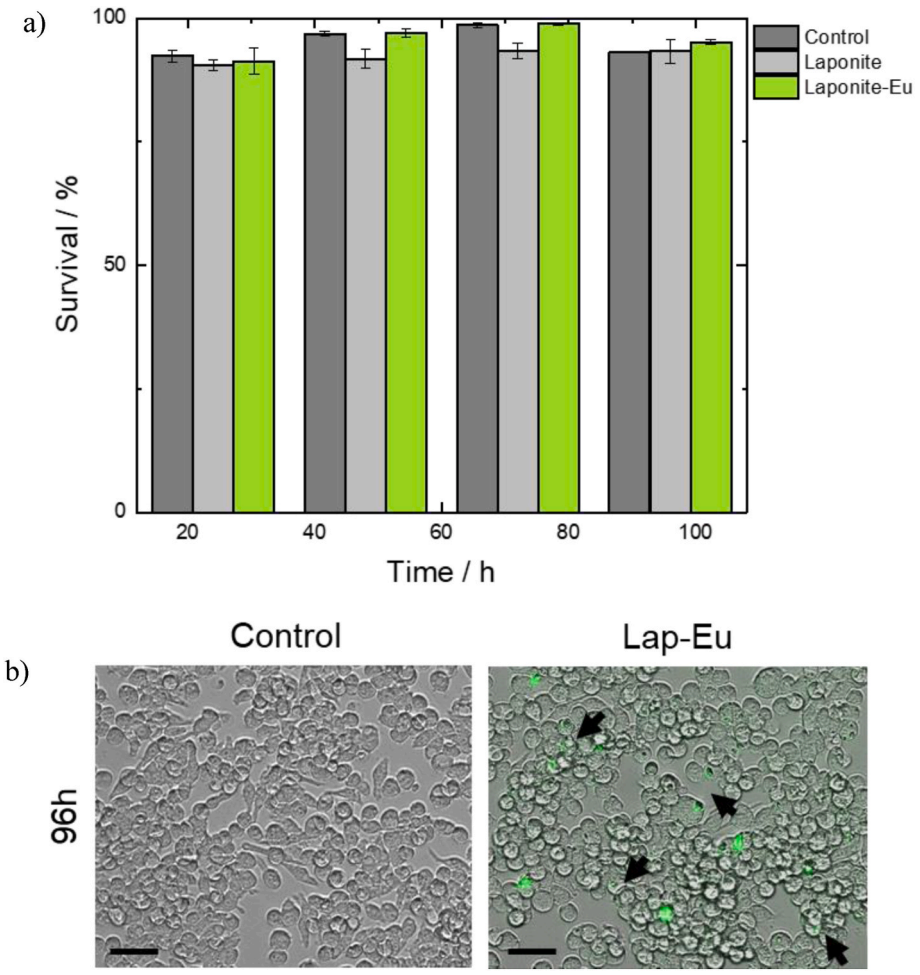

Fig. 7. a) J774 cell survival after 24, 48, 72, and 96 h of Eu-doped Laponite administration compared to control cells treated with Laponite and untreated control cells; and b) Phase-contrast images of control J774 cells (without administration) and cells after 96 h of the administration of Eu-doped Laponite administration.

compared to cells with plain Laponite or Eu-doped Laponite administration.

Fig. 7b illustrates phase-contrast images overlapped with epifluorescence images, demonstrating that cell morphology has not changed after 96 h of exposure. Contrast agents, classically based on gadolinium and manganese, are widely used in magnetic resonance imaging (MRI) as a powerful tool for disease diagnosis. The currently used clinical MRI contrast agents aim to remain in the blood long enough to obtain high-resolution images. Thus, significant efforts are being made to develop new products with easy synthesis methods or cheaper base materials that fulfill these requirements [22]. The combination of active cations intercalated into Laponite particles as a contrast agent could be an alternative to be explored in the future, based on its biocompatibility.

4. Conclusions

In this study, we present a combination of luminescence and confocal Raman spectroscopy to monitor the uptake and internalization of Eu-doped Laponite nanoparticles into the J774 macrophage cell line. Specifically, Eu^{3+} ions acts as a luminescent model of the fluorescent drug, and the nanoclay represents an interesting host matrix for drug delivery systems. The presented strategy allows simultaneous and independent tracking of the delivery nanosystem and the fluorescent cargo. We have demonstrated that it is possible to separately identify the localization of the nanoparticle and Eu^{3+} ions within the cell by acquiring the Raman signal from both the nanoparticle and the cell, along with Eu^{3+} luminescence acquired at the same spot. To confirm the incorporation of the Eu-Laponite system within the cell, rather than potential adhesion to the cell membrane, we captured images at different Z planes. Moreover, it has also been proved that the fluorescent cargo keeps attached to the nanoparticle. Finally, the biocompatibility of the nanoplatforms and their cargo has been studied, revealing no significant differences in the survival rate between control cells and those treated with plain Laponite or Eu^{3+}-doped Laponite.

CRediT authorship contribution statement

Nerea Iturrioz-Rodríguez: Writing – original draft, Investigation, Data curation. **Rosa Martín-Rodríguez:** Writing – review & editing, Supervision, Funding acquisition, Conceptualization. **Fernando Aguado:** Writing – review & editing, Methodology, Formal analysis, Data curation, Conceptualization. **Lorena González-Legarreta:** Methodology, Data curation. **Jesús González:** Data curation. **Rafael Valiente:** Investigation. **Mónica L. Fanarraga:** Investigation. **Ana C. Perdigón:** Writing – review & editing, Supervision, Funding acquisition, Conceptualization.

Acknowledgment

We would like to thank IDIVAL for financial support, Projects Nº INNVAL19/18. This work has been supported by the Spanish MCIN and European Union under Project TED2021-131305B-I00 funded by MCIN/AEI/10.13039/501100011033 and by the European Union -NextGenerationEU/PRTR.

References

[1] S.L. Tawari, D.L. Koch, C. Cohen, Electrical double-layer effects on the Brownian diffusivity and aggregation rate of Laponite clay particles, J. Colloid Interface Sci. 240 (2001) 54–66, https://doi.org/10.1006/jcis.2001.7646.

[2] H. Tomás, C.S. Alves, J. Rodrigues, Laponite®: a key nanoplatform for biomedical applications? Nanomed. Nanotechnol. Biol. Med. 14 (2018) 2407–2420, https://doi.org/10.1016/j.nano.2017.04.016.

[3] M. Gonçalves, P. Figueira, D. Maciel, J. Rodrigues, X. Qu, C. Liu, H. Tomás, Y. Li, PH-sensitive Laponite®/doxorubicin/alginate nanohybrids with improved anticancer efficacy, Acta Biomater. 10 (2014) 300–307, https://doi.org/10.1016/j.actbio.2013.09.013.

[4] S. Wang, F. Zheng, Y. Huang, Y. Fang, M. Shen, M. Zhu, X. Shi, Encapsulation of amoxicillin within laponite-doped poly(lactic-co-glycolic acid) nanofibers: preparation, characterization, and antibacterial activity, ACS Appl. Mater. Interfaces 4 (2012) 6393–6401, https://doi.org/10.1021/am302130b.

[5] H. Jung, H.M. Kim, Y. Bin Choy, S.J. Hwang, J.H. Choy, Itraconazole-Laponite: kinetics and mechanism of drug release, Appl. Clay Sci. 40 (2008) 99–107, https://doi.org/10.1016/j.clay.2007.09.002.

[6] T. Jin, S. Tsutsumi, Y. Deguchi, K. Machida, G. Adachi, Preparation and luminescence characteristics of the europium and terbium complexes incorporated into a silica matrix using a sol-gel method, J. Alloys Compd. 252 (1997) 59–66, https://doi.org/10.1016/S0925-8388(96)02385-7.

[7] K. Binnemans, Lanthanide-based luminescent hybrid materials, Chem. Rev. 109 (2009) 4283–4374, https://doi.org/10.1021/cr8003983.

[8] H. Zeng, X. Li, M. Sun, S. Wu, H. Chen, Synthesis of europium-doped fluorapatite nanorods and their biomedical applications in drug delivery, Molecules 22 (2017) 1–7, https://doi.org/10.3390/molecules22050753.

[9] N. Iturrioz-Rodríguez, R. Martín-Rodríguez, C. Renero-Lecuna, F. Aguado, L. González-Legarreta, J. González, M.L. Fanarraga, A.C. Perdigón, Free-labeled nanoclay intracellular uptake tracking by confocal Raman imaging, Appl. Surf. Sci. 537 (2021) 147870, https://doi.org/10.1016/j.apsusc.2020.147870.

[10] T. Chernenko, F. Buyukozturk, M. Miljkovic, R. Carrier, M. Diem, M. Amiji, Label-free Raman microspectral analysis for comparison of cellular uptake and distribution between nontargeted and EGFR-targeted biodegradable polymeric nanoparticles, Drug Deliv. Transl. Res. 3 (2013) 575–586, https://doi.org/10.1007/s13346-013-0178-3.

[11] J.T. Kloprogge, Raman Spectroscopy of Clay Minerals, first ed., Elsevier Ltd., 2017 https://doi.org/10.1016/B978-0-08-100355-8.00006-0.

[12] M. Pelletier, L.J. Michot, B. Humbert, O. Barrès, J.B. D'Espinose de la Caillerie, J. L. Robert, Influence of layer charge on the hydroxyl stretching of trioctahedral clay minerals: a vibrational study of synthetic Na- and K-saponites, Am. Mineral. 88 (2003) 1801–1808, https://doi.org/10.2138/am-2003-11-1221.

[13] C. Krafft, S.B. Sobottka, G. Schackert, R. Salzer, Near infrared Raman spectroscopic mapping of native brain tissue and intracranial tumors, Analyst 130 (2005) 1070–1077, https://doi.org/10.1039/b419232j.

[14] Z. Movasaghi, S. Rehman, I.U. Rehman, Raman spectroscopy of biological tissues, Appl. Spectrosc. Rev. 42 (2007) 493–541, https://doi.org/10.1080/05704920701551530.

[15] A.C.S. Talari, Z. Movasaghi, S. Rehman, I.U. Rehman, Raman spectroscopy of biological tissues, Appl. Spectrosc. Rev. 50 (2015) 46–111, https://doi.org/10.1080/05704928.2014.923902.

[16] M. Kirsch, G. Schackert, R. Salzer, C. Krafft, Raman spectroscopic imaging for in vivo detection of cerebral brain metastases, Anal. Bioanal. Chem. 398 (2010) 1707–1713, https://doi.org/10.1007/s00216-010-4116-7.

[17] A. Synytsya, P. Alexa, J. de Boer, M. Loewe, M. Moosburger, M. Würkner, K. Volka, Raman spectroscopic study of serum albumins: an effect of proton- and γ-irradiation, J. Raman Spectrosc. 38 (2007) 1646–1655, https://doi.org/10.1002/jrs.1884.

[18] R. Faiman, K. Larsson, Assignment of the C-H stretching vibrational frequencies in the Raman spectra of lipids, J. Raman Spectrosc. 4 (1976) 387–394, https://doi.org/10.1002/jrs.1250040406.

[19] S. Vanden-Hehir, W.J. Tipping, M. Lee, V.G. Brunton, A. Williams, A.N. Hulme, Raman imaging of nanocarriers for drug delivery, Nanomaterials 9 (2019) 1–19, https://doi.org/10.3390/nano9030341.

[20] S. Li, T. Chen, Y. Wang, L. Liu, F. Lv, Z. Li, Y. Huang, K.S. Schanze, S. Wang, Conjugated polymer with intrinsic alkyne units for synergistically enhanced Raman imaging in living cells, Angew. Chemie - Int. Ed. 56 (2017) 13455–13458, https://doi.org/10.1002/anie.201707042.

[21] C. Matthäus, S. Schubert, M. Schmitt, C. Krafft, B. Dietzek, U.S. Schubert, J. Popp, Resonance Raman spectral imaging of intracellular uptake of β-carotene loaded poly(D, L -lactide-co-glycolide) nanoparticles, ChemPhysChem 14 (2013) 155–161, https://doi.org/10.1002/cphc.201200577.

[22] M. Rogosnitzky, S. Branch, Gadolinium-based contrast agent toxicity: a review of known and proposed mechanisms, Biometals 29 (2016) 365–376, https://doi.org/10.1007/s10534-016-9931-7.